Defect Creation by Linker Fragmentation in Metal–Organic Frameworks and Its Effects on Gas Uptake Properties

Gokhan Barin,[†] Vaiva Krungleviciute,[‡,§] Oleksii Gutov,[†] Joseph T. Hupp,[*,†] Taner Yildirim,[*,‡,§] Omar K. Farha[*,†,¶]

[†] *Department of Chemistry, Northwestern University, 2145 Sheridan Road, Evanston, Illinois 60208, USA*

[‡] *NIST Center for Neutron Research, National Institute of Standards and Technology, Gaithersburg, MD 20899, USA*

[§] *Department of Materials Science and Engineering, University of Pennsylvania, Philadelphia, PA 19104, USA*

[¶] *Department of Chemistry, Faculty of Science, King Abdulaziz University, Jeddah, Saudi Arabia*

** Email: j-hupp@northwestern.edu, taner@seas.upenn.edu, o-farha@northwestern.edu*

SUPPORTING INFORMATION

Table of Contents

1. General Methods

All air- or water-sensitive reactions were carried out under a dry nitrogen atmosphere using standard Schlenk techniques. Unless otherwise stated, all chemicals and solvents were purchased from Sigma-Aldrich Co. (Milwaukee, WI) and used without further purification. Linker **L** and **NU-125** were prepared[1] following procedures reported in the literature. Analytical thin-layer chromatography (TLC) was performed on aluminum sheets, precoated with silica gel 60-F_{254} (Merck 5554). Flash column chromatography was carried out using silica gel 60 (Silicycle) as the stationary phase. Water was obtained from a deionized water source provided by Northwestern University. Deuterated solvents were purchased from Cambridge Isotope Laboratories (Andover, MA) and used without further purification.

^{1}H and ^{13}C NMR spectra were recorded on a Bruker 500 FT-NMR spectrometer (499.773 MHz for ^{1}H and 125.669 MHz for ^{13}C) and ^{19}F NMR spectra were recorded on an Agilent 400 NMR spectrometer (376.113 MHz for ^{19}F) at ambient temperature. ^{1}H NMR data are reported as follows: chemical shift (multiplicity (br s = broad singlet, s = singlet, d = doublet, dd = doublet of doublets, ddd = doublet of doublets of doublets, t = triplet, q = quartet, and m = multiplet), integration, and coupling constants). Chemical shifts are reported in ppm relative to the signals corresponding to the residual non-deuterated solvents. Electrospray Ionization (ESI) mass spectra were obtained on an Agilent 6210 LC-TOF high-resolution mass spectrometer.

Powder patterns were collected on a Bruker AXS APEX2 diffractometer equipped with a CCD detector and a CuKα IμS microfocus source with MX optics. Samples were loaded into glass capillaries with a small amount of mother liquor, and mounted on a goniometer head. Data were collected with an area detector as rotation frames over 180° in φ at 2θ values of 12°, 24°, and 36° and exposed for 10 min for each frame. At a distance of 150 mm, the detector area covers 24° in 2θ. Overlapping sections of data were matched and the resulting pattern integrated using the Bruker APEX2 Phase ID program. Powder pattern data were treated for amorphous background scatter (EVA 16, Copyright Bruker-AXS 1996-2010).

Nitrogen isotherms measured at Northwestern University were carried out on an ASAP 2020 (Micromeritics) and those measured at NIST were carried out on an Autosorb-1MP instrument (Quantachrome Instrument). Measurements were performed at 77 K and the temperature was held constant using a liquid N_2 bath.

All high-pressure isotherm measurements were performed at the NIST Center for Neutron Research using a computer controlled Sieverts apparatus, details of which have been published elsewhere. All samples were thoroughly outgassed to remove residual solvents and sample handling was performed in a helium glove box. All gases were of Research or Scientific grade, with a minimum purity of 99.999%.

2. Synthesis

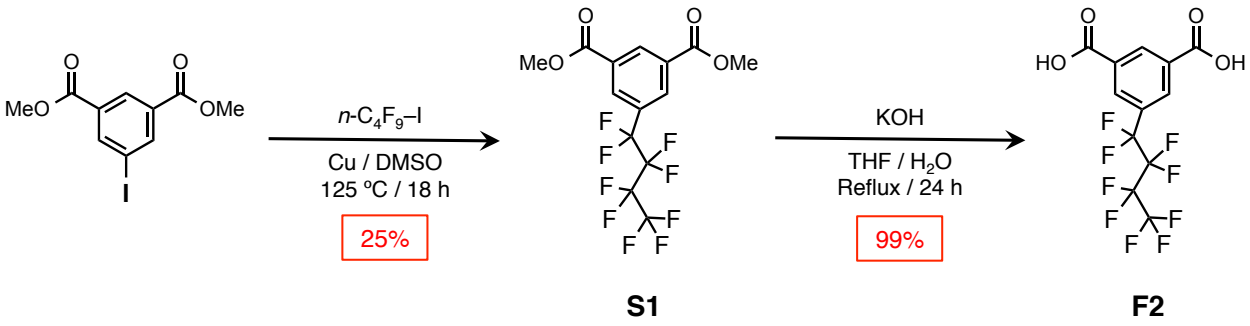

Scheme S1. Synthesis of fragment **F2**

Synthesis of S1: The procedure was adopted from a literature report.[2] A suspension of Cu powder (2.8 g, 44.0 mmol) in anhydrous DMSO (25 mL) was heated at 125 ºC for 15 min under nitrogen, and followed by the dropwise addition of perfluorobutyl iodide (5.6 g, 16.2 mmol) over 10 min. After 45 min, dimethyl 5-iodoisophthalate (4.0 g, 12.5 mmol) dissolved in anhydrous DMSO (10 mL) was added dropwise and the resulting mixture was stirred at 125 ºC for 18 h. After cooling to RT, the reaction was quenched with cold water (200 mL) and diethyl ether was added (300 mL). The mixture was filtered through celite, and then the aqueous phase was extracted with diethyl ether (2 x 100 mL). The combined organic phases were dried over Na_2SO_4. After removing the solvent under vacuum, the crude product was subjected to column chromatography (SiO_2, Hexanes/EtOAc, 20:1) affording **S1** as a white solid (1.3 g, 25%). ^{1}H NMR ($CDCl_3$, 500 MHz, 298 K): δ = 8.90 (t, *J* = 1.5 Hz, 1H), 8.45 (d, *J* = 1.5 Hz, 2H), 4.00 (s, 6H); ^{19}F NMR ($CDCl_3$, 375 MHz, 298 K): δ = –81.0 (3F), –111.0 (2F), –122.4 (2F), –125.5 (2F); ^{13}C NMR ($CDCl_3$, 125 MHz, 298 K): δ = 164.92, 133.98, 132.04, 131.99, 131.94, 131.64, 130.25, 130.06, 129.86, 52.87; HRMS (EI) *m/z* calcd 412.0357 for $C_{14}H_9O_4F_9$, found 412.0352 $[M]^+$.

Synthesis of F2: Compound **S1** (1.3 g, 3.2 mmol) was dissolved in THF (50 mL) and a solution of KOH (6.6 g, 118 mmol) in H_2O (150 mL) was added. The resulting biphasic solution was stirred vigorously at 80 ºC for 24 h. After cooling the reaction mixture to room temperature, THF was removed *in vacuo* and the remaining aqueous solution was acidified to pH < 2 using concentrated HCl. The resulting precipitate was collected by vacuum filtration, washed with H_2O, and dried for 24 h under vacuum to afford **F2** as a white solid (1.2 g, 99%). ^{1}H NMR

(DMSO-d_6, 500 MHz, 298 K): δ = 13.88 (br s, 2H), 8.72 (t, J = 1.5 Hz, 1H), 8.33 (d, J = 1.5 Hz, 2H); ^{19}F NMR (DMSO-d_6, 375 MHz, 298 K): δ = –80.5 (3F), –110.2 (2F), –122.4 (2F), –125.2 (2F); ^{13}C NMR (DMSO-d_6, 125 MHz, 298 K): δ = 165.18, 133.72, 132.86, 130.71, 130.67, 130.62, 128.35, 128.15, 127.96; HRMS (ESI) *m/z* calcd 382.9971 for $C_{12}H_4O_4F_9$, found 382.9976 $[M - H]^-$.

3. Syntheses and Characterization of Mixed Linker-Fragment MOFs

3.1. NU-125-F1

Synthesis: A mixture of $Cu(NO_3)_2 \cdot 2.5H_2O$ (50 mg, 215 μmol), linker **L** (20 mg, 26 μmol), and fragment **F1** (*x* mg, see table below) was dissolved in DMF (5 mL). 3 drops of concentrated HBF_4 were then added to this mixture and sonicated for 5 min. This solution was divided into two 2-dram vials (VWR, catalog #66011-085). The vials were capped and placed into an oven at 80 ºC for 24 h. The resulting teal crystalline powder was combined and washed thoroughly with DMF. The crystalline sample was immersed in DMF (20 mL) for further 24 h to ensure the removal of unreacted ligands.

Feed Ratio (F1 : L)	**Amount of F1 (*x* mg)**
1:1	4.4
2:1	8.8
3:1	13.2
4:1	17.6
5:1	22.0
10:1	43.0
15:1	64.5
20:1	86.0

Powder X-Ray Diffraction (PXRD): Phase purities of bulk materials obtained from various feed ratios were determined (Figure S1) by PXRD. The resulting PXRD patterns were compared to that of **NU-125**, which is the parent framework made solely from the linker **L**. Accordingly, the feed ratio of 3:1 provides the maximum incorporation of fragment while maintaining the structure of the parent framework **NU-125**.

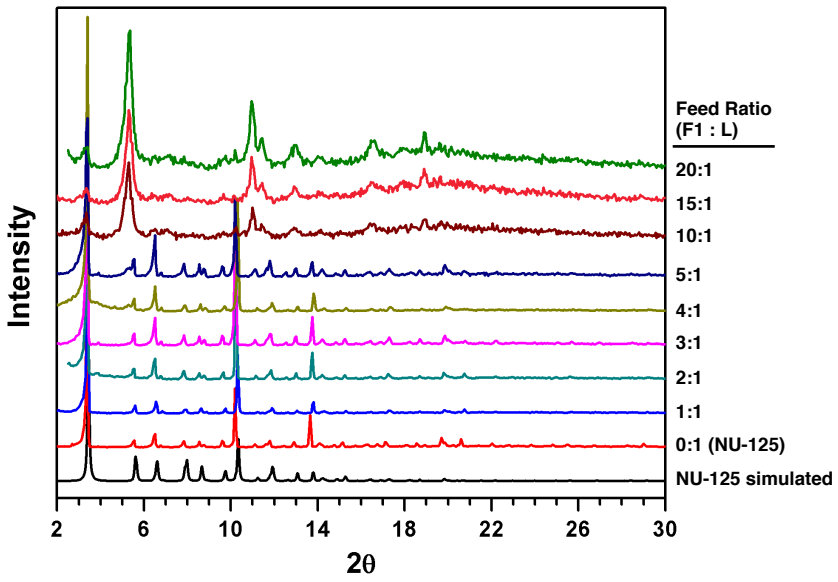

Figure S1. PXRD patterns of **NU-125-F1** of varying fragment to linker ratios.

^{1}H NMR Spectroscopy: The incorporation amount of fragment into the parent framework was determined (Figure S2) using ^{1}H NMR spectroscopy. The crystals were digested in DMSO-d_6/DCl mixture. The plot in Figure S2d demonstrates that the fragment amount in the crystals is gradually increased upon increasing the feed ratio in solution.

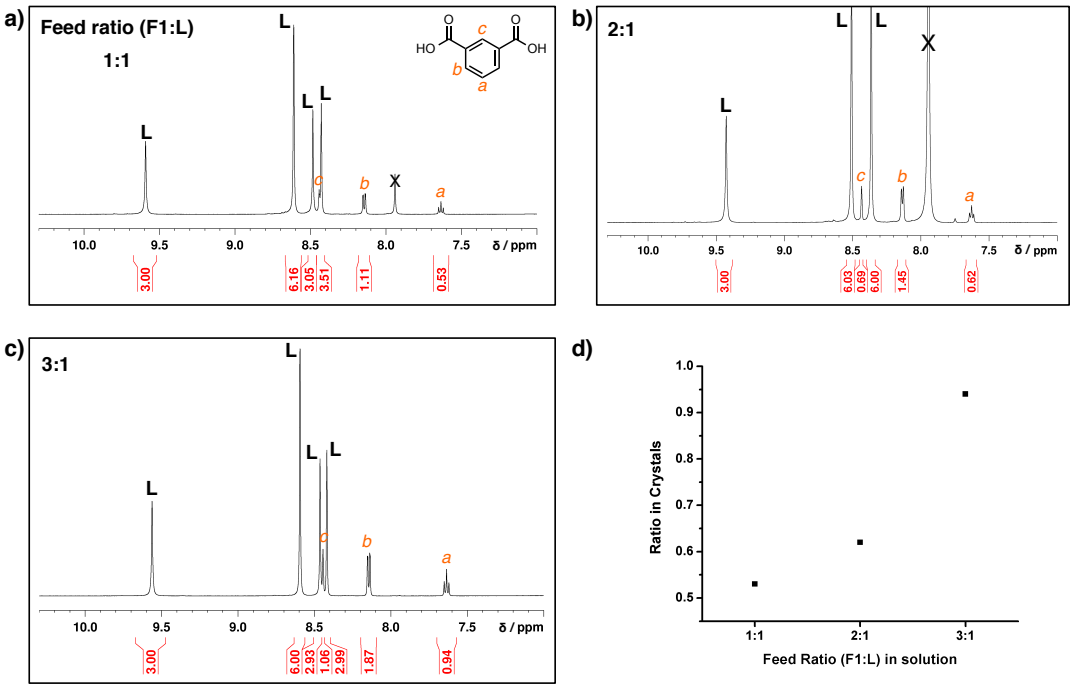

Figure S2. (a-c) ^{1}H NMR spectra of crystals (feed ratio from 1:1 to 3:1) digested in DMSO-d_6/DCl. The ratios of fragment **F1** and linker **L** in the resulting mixed linker-fragment MOFs were determined using the integrations of the peaks. (d) The plot demonstrates the increasing incorporation of fragment into the crystals as the feed ratio is increased in solution. (X denotes the residual solvent (DMF) peak.)

3.2. NU-125-F2

Synthesis: A mixture of $Cu(NO_3)_2 \cdot 2.5H_2O$ (50 mg, 215 μmol), linker **L** (20 mg, 26 μmol), and fragment **F2** (*x* mg, see table below) was dissolved in DMF (5 mL). 3 drops of concentrated HBF_4 were then added to this mixture and sonicated for 5 min. This solution was divided into two 2-dram vials (VWR, catalog #66011-085). The vials were capped and placed into an oven at 80 ºC for 24 h. The resulting teal crystalline powder was combined and washed thoroughly with DMF. The crystalline sample was immersed in DMF (20 mL) for further 24 h to ensure the removal of unreacted ligands.

Feed Ratio (F2 : L)	**Amount of F2 (*x* mg)**
1:1	10
2:1	20
3:1	30
4:1	40
5:1	50

Synthesis of Fragment (F2) only MOF: A mixture of $Cu(NO_3)_2 \cdot 2.5H_2O$ (50 mg, 215 μmol) and fragment **F2** (30 mg, 78 μmol) was dissolved in DMF (5 mL). 3 drops of concentrated HBF_4 were then added to this mixture and mixed well. This solution was divided into two 2-dram vials (VWR, catalog #66011-085). The vials were capped and placed into an oven at 80 ºC for 24 h. The resulting teal crystalline powder was combined and washed thoroughly with DMF.

Powder X-Ray Diffraction: Similar to **NU-125-F1**, phase purities of bulk materials were determined by PXRD as shown in Figure S3. In this case, however, we have determined that the optimal feed ratio in solution was 2:1 (**F2**:**L**), which was isostructural to the parent framework **NU-125**. As a control experiment, we also prepared the crystalline material made from the only fragment component (1:0, **F2**:**L**) in order to ensure that the resulting mixed linker-fragment MOFs are not a mixture of two different phases. Indeed, the fragment itself was found to form (Figure S3, top) a structure different than the parent material.

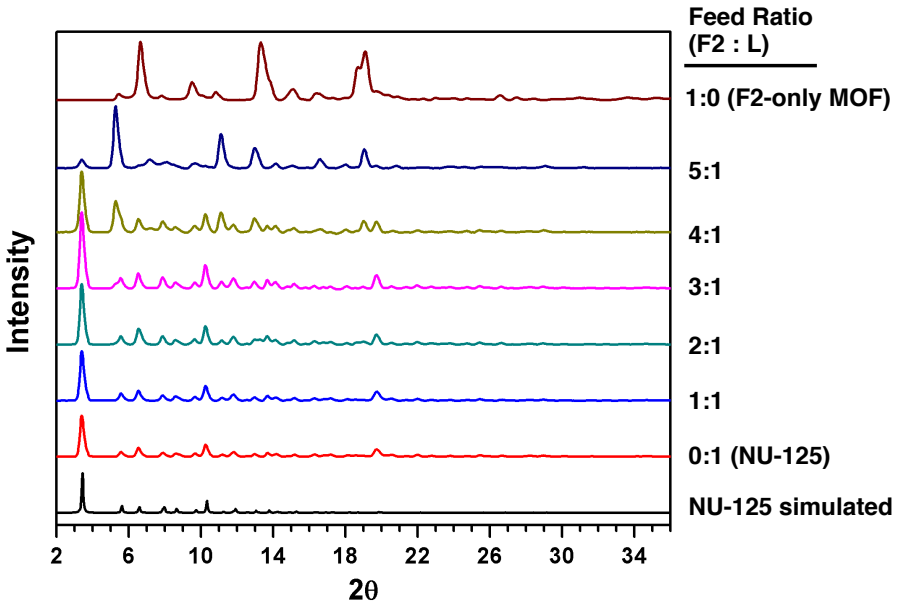

Figure S3. PXRD patterns of **NU-125-F2** of varying fragment to linker ratios.

^{1}H and ^{19}F NMR Spectroscopy: The crystalline powder materials were digested in DMSO-d_6/DCl mixture and analyzed (Figure S4) by ^{1}H NMR spectroscopy in order to determine the ratio between the fragment **F2** and the linker **L** in the resulting crystals. ^{19}F NMR spectroscopy was used (Figure S5) to provide further evidence for the presence of fluorinated fragment.

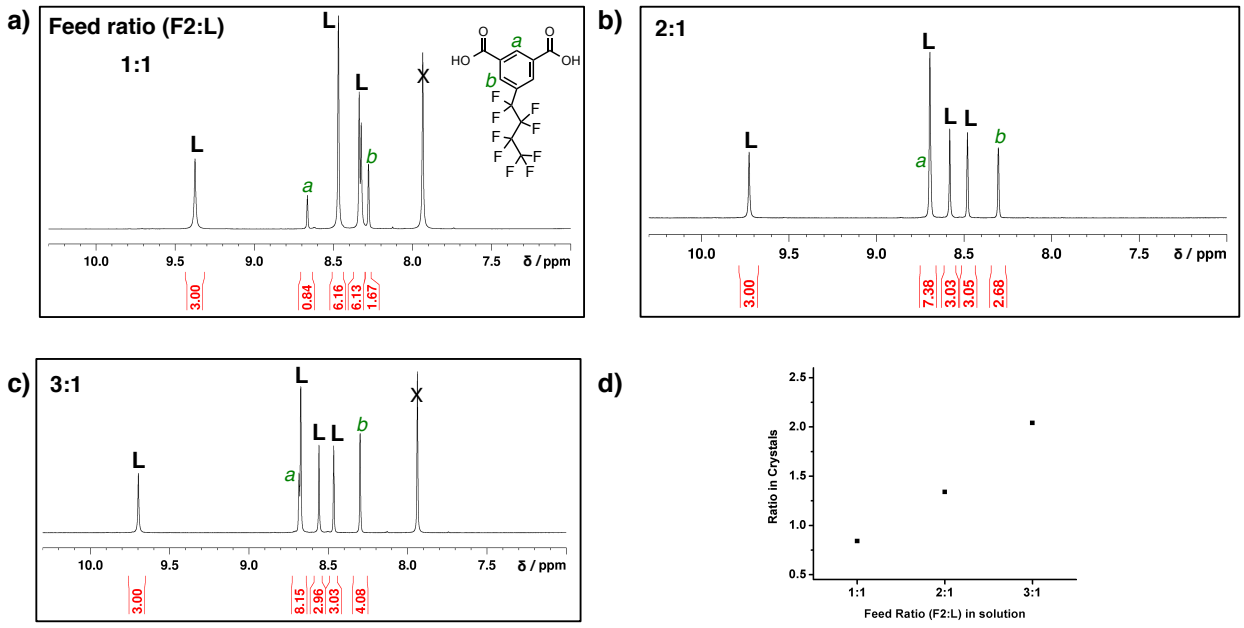

Figure S4. (a-c) ^{1}H NMR spectra of crystals (feed ratio from 1:1 to 3:1) digested in DMSO-d_6/DCl. The ratios of fragment **F2** and linker **L** in the resulting mixed linker-fragment MOFs were determined using the integrations of the peaks. (d) The plot demonstrates the increasing incorporation of fragment into the crystals as the feed ratio is increased in solution. (X denotes the residual solvent (DMF) peak.)

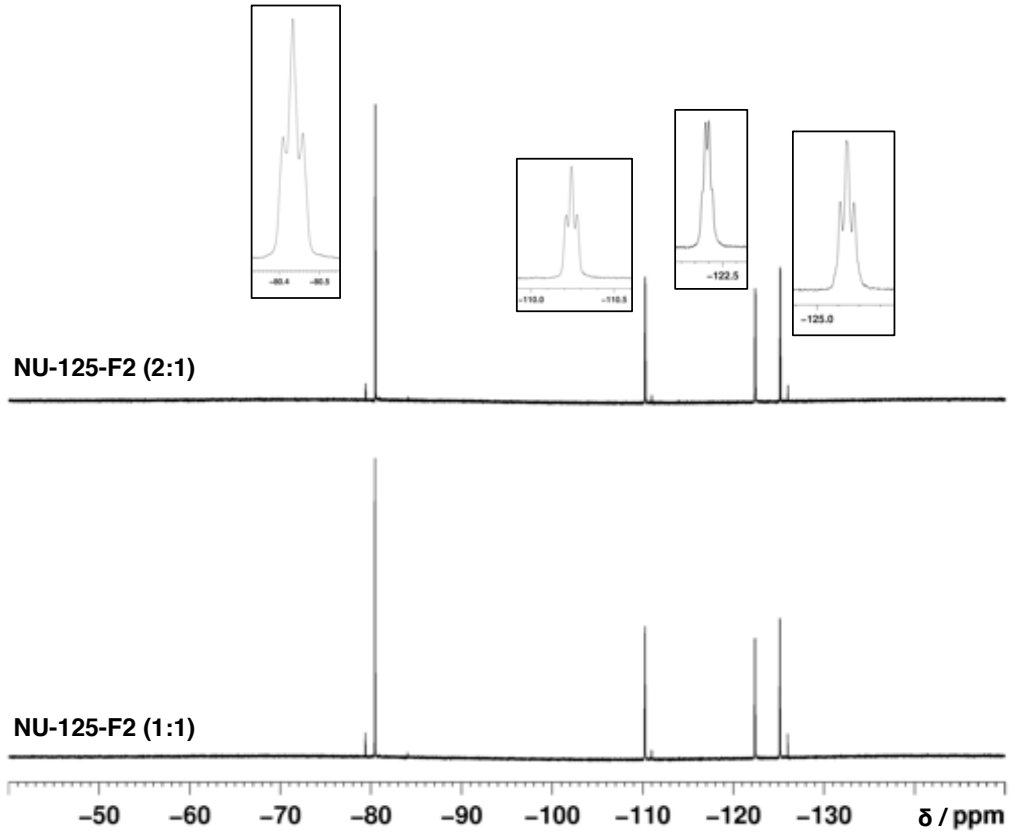

Figure S5. ^{19}F NMR spectra of **NU-125-F2** crystals obtained from 1:1 and 2:1 feed ratios in DMSO-d_6/DCl.

Surface Adsorption of Fragments on the Parent Structure (NU-125):

In order to confirm that fragments are indeed incorporated into the framework and to rule out the possibility of surface adsorption of **F1** and **F2** on the parent framework **NU-125**, we carried out the control experiment in which the crystals of **NU-125** were soaked into a 50 mM solution of **F1** and **F2** in DMF and kept at 80 ºC for 24 h. After washing the crystals thoroughly with DMF, ^{1}H NMR spectra of digested crystals in DMSO-d_6/DCl were obtained. In both cases, only the peaks from linker **L** were observed (Figure S6), indicating no incorporation or surface adsorption of fragments to the parent framework **NU-125**. This result also confirms that even if there were fragments attached on the surface of crystals for **NU-125-F1** and **NU-125-F2**, they are removed completely by washing with excess DMF.

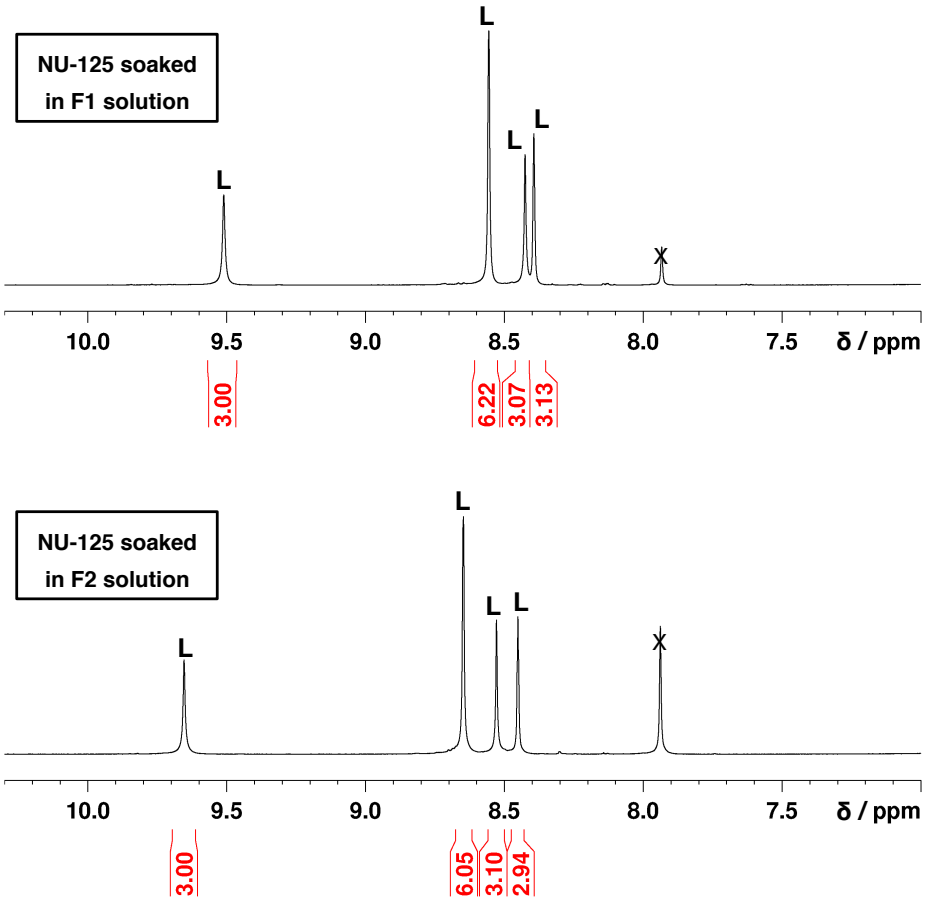

Figure S6. ^{1}H NMR spectra of **NU-125** crystals, after soaking into a DMF solution of **F1** (top) and **F2** (bottom), in DMSO-d_6/DCl. (X denotes the residual solvent (DMF) peak.)

3.3. HKUST-1-F1

Synthesis: $Cu(NO_3)_2 \cdot 2.5H_2O$ (165 mg, 708 μmol), benzene-1,3,5-tricarboxylic acid **btc** (50 mg, 238 μmol), and fragment **F1** (*x* mg, see table below) were added to a 4-dram vial (VWR, catalog #66011-121), followed by the addition of DMF (7 mL) and concentrated HBF_4 (0.3 mL). The mixture was sonicated for 15 min and then placed into an oven at 80 ºC for 20 h. The resulting teal crystalline material was washed with DMF thoroughly.

Feed Ratio (F1 : btc)	Amount of F1 (*x* mg)
1:1	40
2:1	80
10:1	400

Powder X-Ray Diffraction: Phase purities of bulk materials of different feed ratios were obtained (Figure S7) by PXRD and the ratio of 2:1 (**F1**:**btc**) was determined to be optimal for the incorporation of **F1** into **HKUST-1** parent framework.

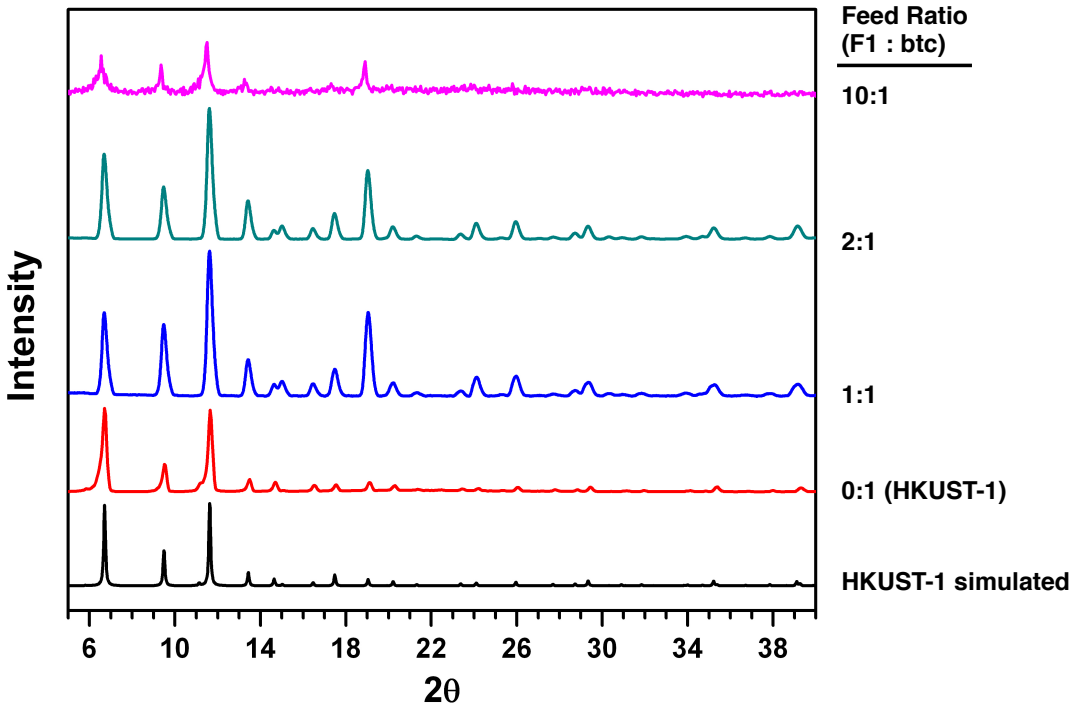

Figure S7. PXRD patterns of **HKUST-1-F1** of varying fragment to linker ratios.

^{1}H NMR Spectroscopy: The crystals of **HKUST-1-F1** were digested in DMSO-d_6/DCl and the incorporation of **F1** was determined using the integration of **btc** and **F1** peaks.

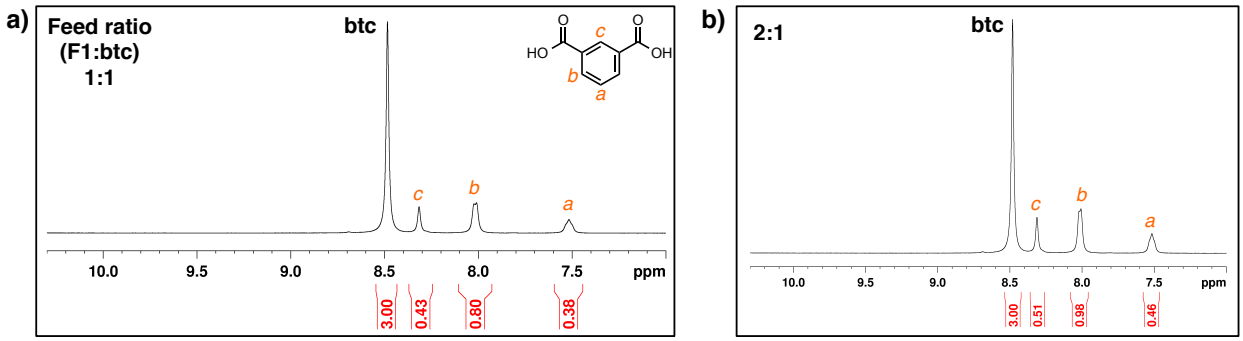

Figure S8. ^{1}H NMR spectra of **HKUST-1-F1** crystals of feed ratio (a) 1:1 and (b) 2:1 digested in DMSO-d_6/DCl.

4. Activation of MOFs

NU-125-F1 and NU-125-F2: After the characterization and scale-up synthesis of **NU-125-F1** (feed ratio 3:1) and **NU-125-F2** (feed ratio 2:1), both MOFs were evacuated using thermal activation after solvent exchange. Both as-synthesized samples were immersed in MeOH for 2 days, during which the soaking solution was replaced every 24 h. Afterwards, MeOH was replaced with CH_2Cl_2 and samples were allowed to sit for 2 more days. The solvent (CH_2Cl_2) was refreshed every 12 h during this period. Solvent-exchanged samples were, first of all, evacuated under vacuum at 30 ºC for 2 h. The temperature was then raised to 110 ºC over 3 h and held at 110 ºC for 18 h. The whole evacuation process was carried out using the degassing port in ASAP 2020. The color of both samples turned into deep purple after activation. The activated samples were stored inside an inert-atmosphere glovebox until further analysis.

HKUST-1-F1: As-synthesized **HKUST-1-F1** sample (feed ratio 2:1) was washed with EtOH three times and kept in EtOH for 24 h. Then, the extract was decanted and the solvent was soaked into acetone for 24 h. Acetone-exchanged **HKUST-1-F1** was evacuated under vacuum at 30 ºC for 1 h. The temperature was then raised to 140 ºC over 3 h and held at 140 ºC for 18 h using the degassing port in ASAP 2020. The activated sample was stored inside an inert-atmosphere glovebox until further analysis.

5. Nitrogen Adsorption Isotherms

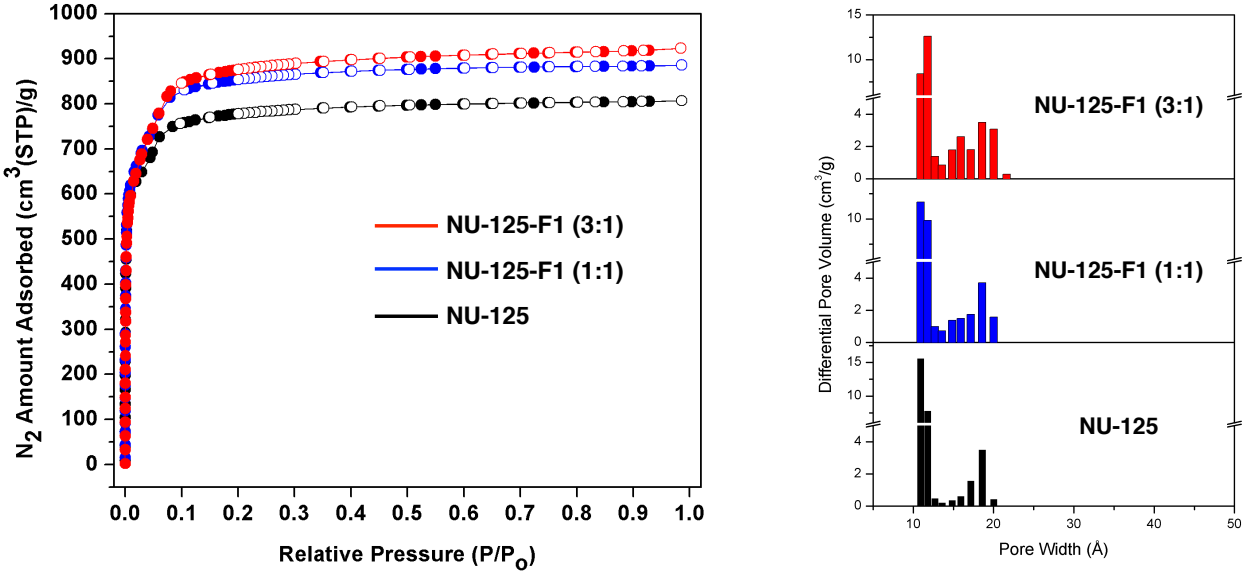

Figure S9. N_2 isotherms of **NU-125** (black) and **NU-125-F1** at feed ratios (**F1**:**L**) of 1:1 (blue) and 3:1 (red) at 77 K. Closed and open symbols represent adsorption and desorption branches, respectively. The total uptake of N_2 increases as the incorporation of fragment **F1** increases. The pore size distributions of corresponding MOFs were determined using density functional theory (DFT). (Measured at Northwestern University)

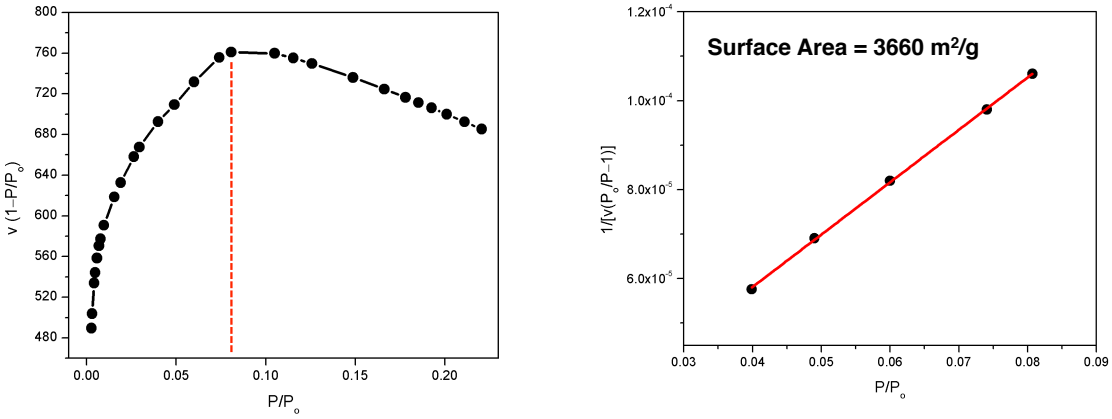

Figure S10. Consistency plot (left) and BET fitting (right) for N_2 isotherm of **NU-125-F1** (3:1), which was used in the high-pressure gas uptake measurements. Only the range below P/P_0 = 0.081 satisfies the first consistency criterion for the application of the BET theory.[3]

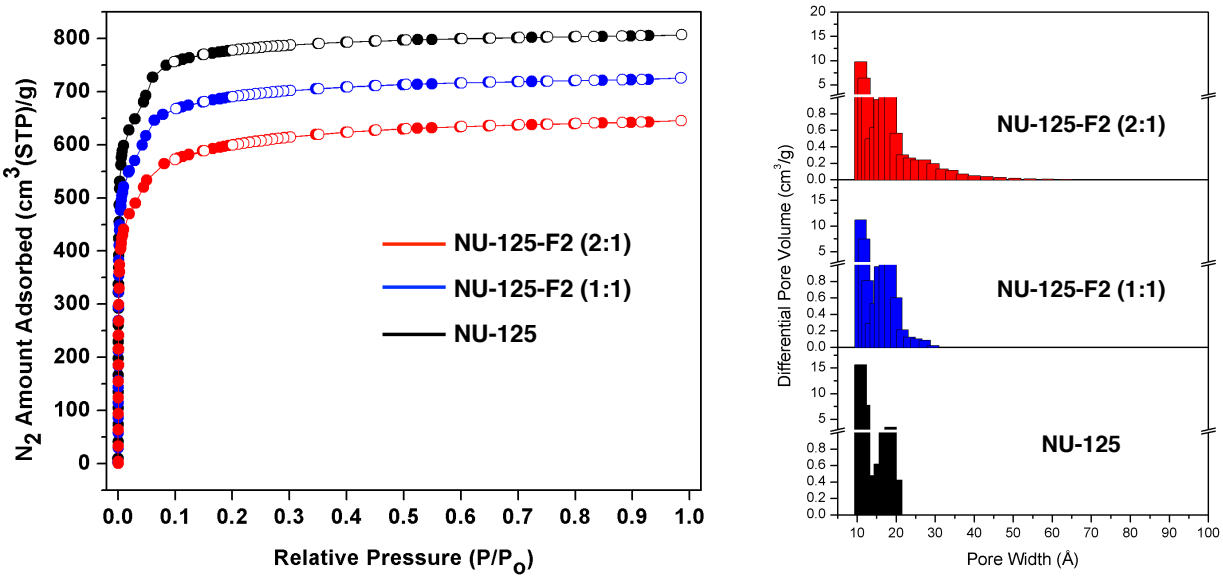

Figure S11. N_2 isotherms of **NU-125** (black) and **NU-125-F2** at feed ratios (**F2**:**L**) of 1:1 (blue) and 2:1 (red) at 77 K. Closed and open symbols represent adsorption and desorption branches, respectively. The total uptake of N_2 decreases as the incorporation of fragment **F2** increases. The pore size distributions of corresponding MOFs were determined using density functional theory (DFT). (Measured at Northwestern University)

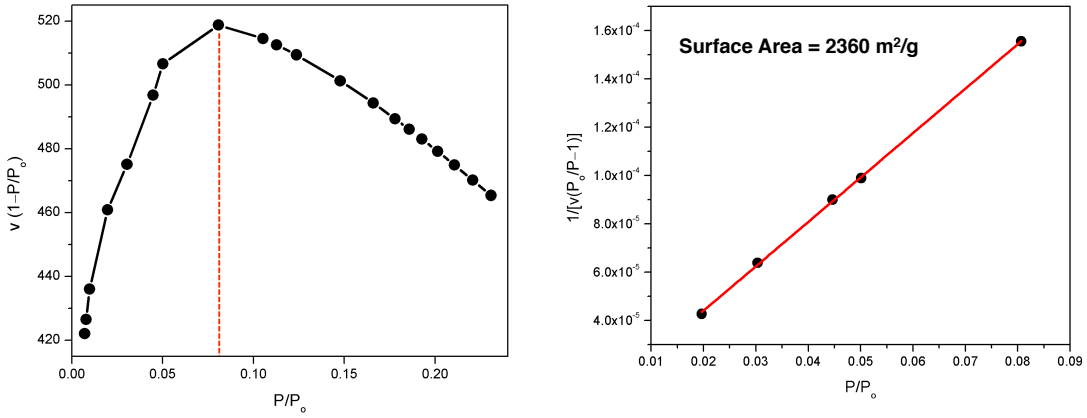

Figure S12. Consistency plot (left) and BET fitting (right) for N_2 isotherm of **NU-125-F2** (2:1), which was used in the high-pressure gas uptake measurements. Only the range below P/P_0 = 0.081 satisfies the first consistency criterion for the application of the BET theory.[3]

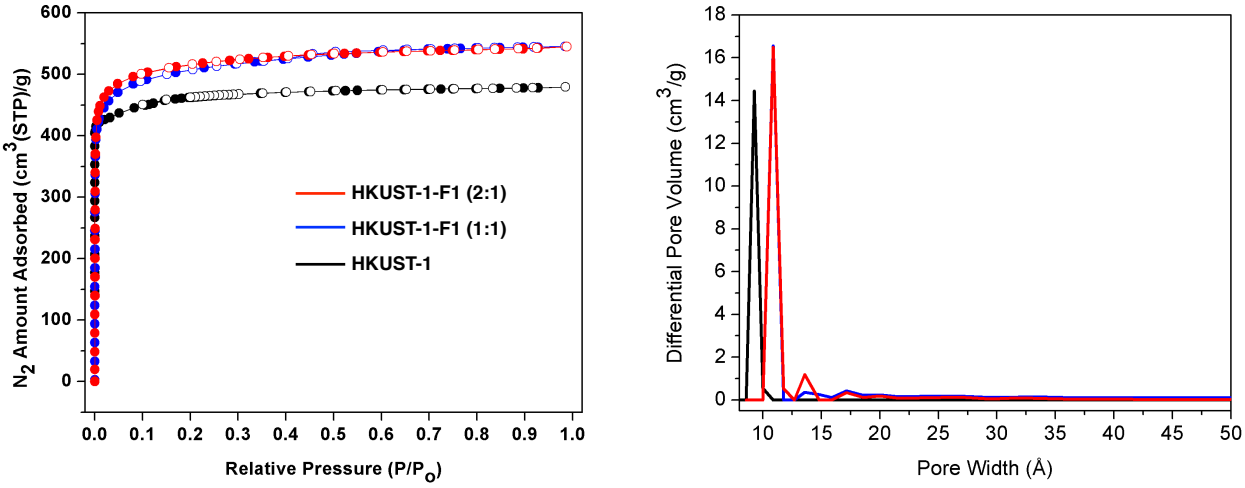

Figure S13. N_2 isotherms of **HKUST-1** (black) and **HKUST-1-F1** at feed ratios (**F1**:**btc**) of 1:1 (blue) and 2:1 (red) at 77 K. Closed and open symbols represent adsorption and desorption branches, respectively. The total uptake of N_2 increases upon incorporation of fragment **F1** when compared to bare **HKUST-1**. The pore size distributions of corresponding MOFs were determined using density functional theory (DFT). (Measured at Northwestern University)

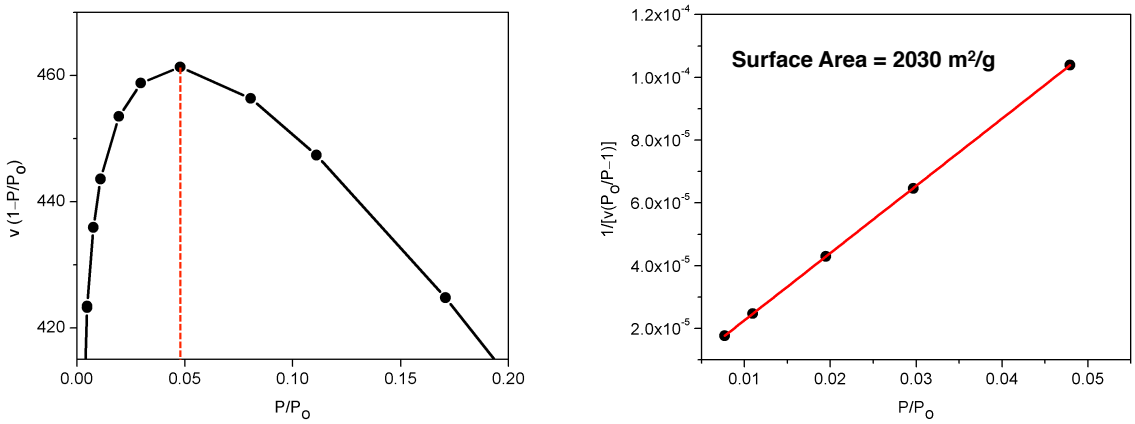

Figure S14. Consistency plot (left) and BET fitting (right) for N_2 isotherm of **HKUST-1-F1** (2:1), which was used in the high-pressure gas uptake measurements. Only the range below P/P_0 = 0.048 satisfies the first consistency criterion for the application of the BET theory.[3]

6. Simulations of Defects in HKUST-1-F1 and NU-125-F1

We have carried out simple PLATON pore volume and BET surface area calculations using nonorthoSA[4] on linker fragmented **HKUST-1** and **NU-125**. In the case of **HKUST-1**, we calculated surface areas and pore volumes for parent **HKUST-1**, **HKUST-1** with one $Cu_2(CO_2)_4$ cluster missing (one defect), and **HKUST-1** with two $Cu_2(CO_2)_4$ clusters missing (two defects) in the conventional unit cell which has 24 $Cu_2(CO_2)_4$ clusters. The removal of one $Cu_2(CO_2)_4$ cluster corresponds to removal of four **btc** linkers and addition of four **F1** fragments. The table below summarizes calculated values for parent and defective **HKUST-1**.

	HKUST-1	**HKUST-1-F1 (one defect)**	**HKUST-1-F1 (two defects)**
Formula	$C_{192}H_{96}[Cu_2(CO_2)_4]_{24}$	$C_{192}H_{100}[Cu_2(CO_2)_4]_{23}$	$C_{192}H_{104}[Cu_2(CO_2)_4]_{22}$
Density (g/cm^3)	0.883	0.8557	0.8284
F1:**btc** ratio in crystal (calcd.)	0:32	4:28 (0.14)	8:24 (0.33)
V_{pore} calcd. (cc/g)	0.78	0.81	0.8426
S_{BET} calcd. (m^2/g)	2063	2233	2307
V_{pore} exp. (cc/g)	*0.78*	*NA*	*0.85*
S_{BET} exp. (m^2/g)	*1850*	*NA*	*2035*

From the table shown above, we can assume that we have two defects (i.e., two $Cu_2(CO_2)_4$ paddlewheels are missing in the conventional **HKUST-1** unit cell which originally has 24 paddlewheel units) since the experimental pore volume of our **HKUST-1-F1** sample (0.85 cc/g) is in good agreement with this model (0.8426 cc/g). Experimental and calculated pore volumes for parent **HKUST-1** are also in excellent agreement. The BET surface areas are overestimated by ~10% in both in parent and defective **HKUST-1**.

Assuming the defect concentration above is correct; we can now estimate the volumetric methane uptake in **HKUST-1-F1**. Using the calculated density of 0.8284 g/cm^3, the gravimetric working capacity of 0.154 g/g translates into a volumetric working capacity of 178 cc/cc. For reference, the volumetric working capacity of parent **HKUST-1** is 190 cc/cc.

We have employed similar calculations on **NU-125** conventional unit cell. We started removing the linker **L** and replacing them with **F1** fragment in the unit cell. For each **L** removed, three **F1** units are included. The parent **NU-125** unit cell has 16 **L**, and therefore, when four linkers are removed, the final composition consists of 12 **L** and 12 **F1**, resulting in a 1:1 ratio. Note that no copper-paddlewheels are removed in this case. Only the linker is fragmented and missing linkages occur between the paddlewheel units. The table below shows the calculated and experimental results for parent **NU-125** and defective **NU-125-F1**.

	NU-125	**NU-125-F1**
Formula	$(C_{36}H_{15}N_9O_{12})_{16}(Cu_2)_{24}$	$(C_{36}H_{15}N_9O_{12})_{12}(C_8H_4O_4)_{12}(Cu_2)_{24}$
Density (g/cm^3)	0.578	0.522
F1:**L** ratio in crystal (calcd.)	0:16	12:12 (1:1)
V_{pore} calcd. (cc/g)	1.29	1.52
S_{BET} calcd. (m^2/g)	3680	3868
V_{pore} exp. (cc/g)	*1.30*	*1.45*
S_{BET} exp. (m^2/g)	*3225*	*3680*

Based on the good agreement between the experimental and calculated pore volumes for our **NU-125** and **NU-125-F1** samples, we can assume that our **NU-125-F1** sample has a final 1:1 ratio of fragment and linker. In fact, that ratio determined by ^{1}H NMR spectroscopy (0.95:1) agrees very well with this model. In both cases, the BET surface area is overestimated by nonorthoSA[4] consistently.

7. Volumetric High-Pressure Adsorption Measurements

The high-pressure isotherms were measured by a custom built, fully computer-controlled Sieverts apparatus as discussed in detail elsewhere.[5-6] Samples were synthesized and activated at NU. In order to make sure the samples are not exposed to air during shipment, we first measured nitrogen isotherms at 77 K (using the same Sievert apparatus) before any high-pressure measurements were taken as a standard protocol. As shown in Figure S15 and S16, the measured pore volumes and surface areas of the samples are in excellent agreement with those measured at NU. The total (i.e., absolute) isotherms shown in Figure S17–S22 were obtained from the

measured excess isotherms by adding amount of gas in the pore volume at the measured pressure and temperature (using NIST MBWR real gas equation). We used the pore volume measured by the nitrogen isotherm, which was confirmed to be same as the pore volume from methane isotherm.

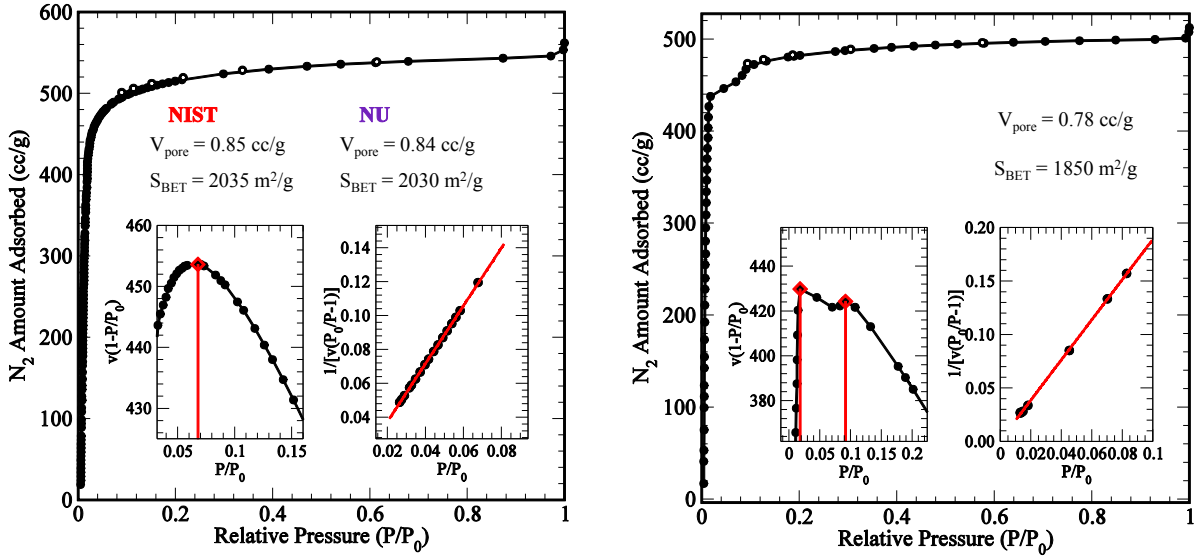

Figure S15. N_2 isotherms for **HKUST-1-F1** (left) and the control sample parent **HKUST-1** (right). The inset shows the consistency plots and the corresponding BET fittings.[3] The calculated pore volume and surface areas are also given and in excellent agreement with the measurements performed at NU (on the same samples).

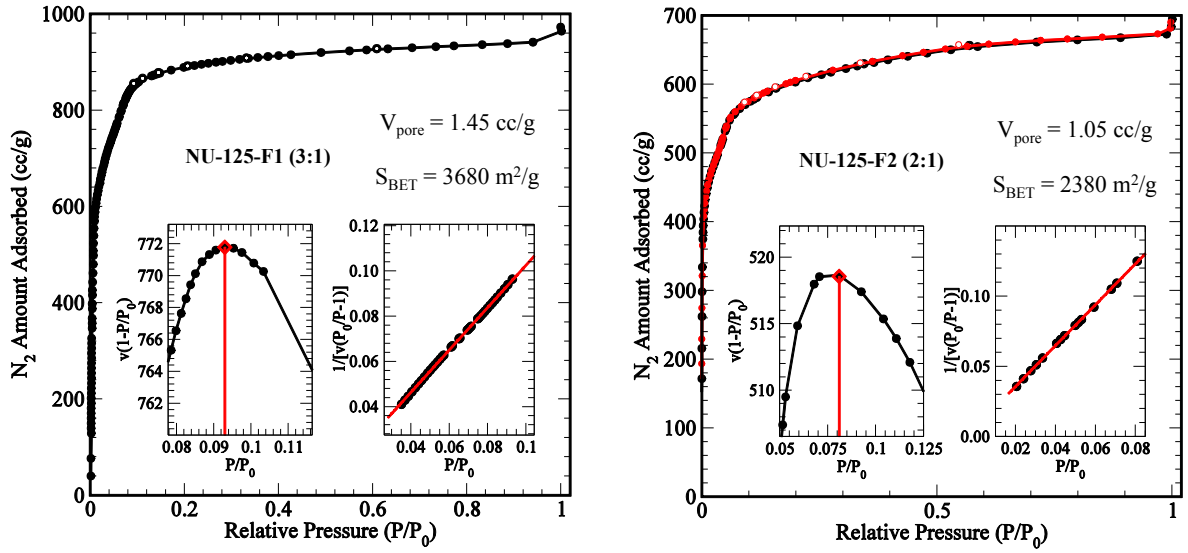

Figure S16. N_2 isotherms for **NU-125-F1** (left) and **NU-125-F2** (right). The inset shows the consistency plots and the corresponding BET fittings.[3] The calculated pore volume and surface areas are also given and in excellent agreement with the measurements performed at NU (on the same samples).

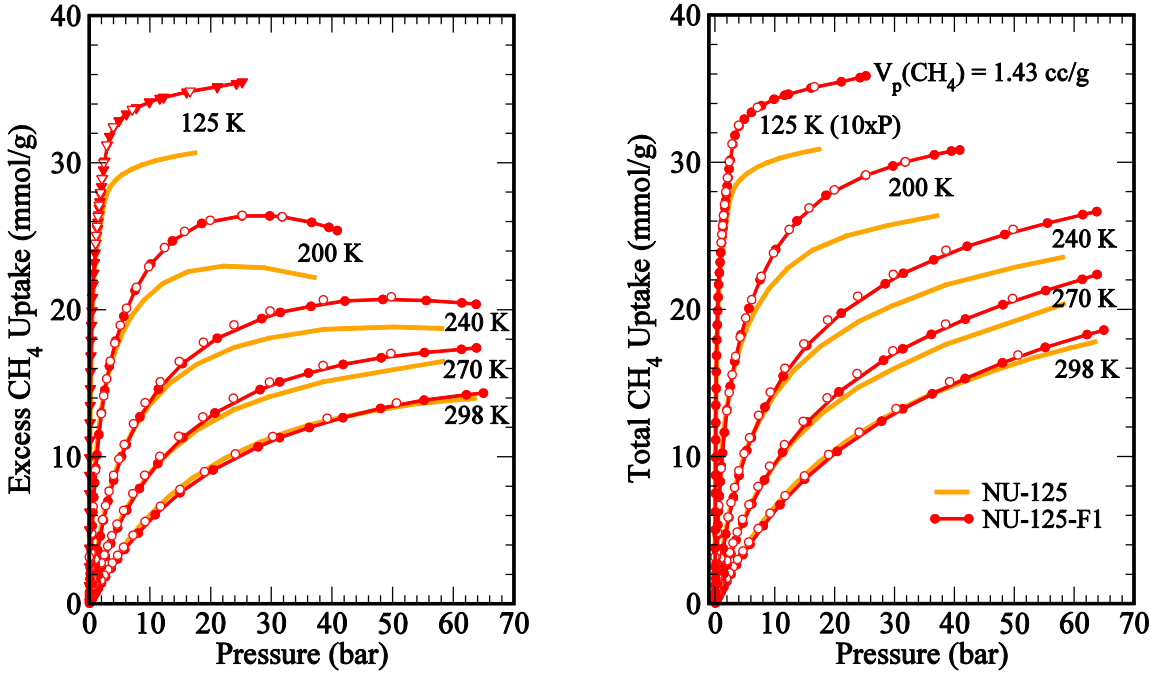

Figure S17. The gravimetric excess (left) and total (right) CH_4 isotherms at various temperatures for **NU-125-F1**. The solid and open points are adsorption and desorption isotherms using calibrated empty cell (EC) cold volumes, respectively. The orange lines are the isotherms from parent **NU-125**. The pressure axes for the 125 K methane isotherms were scaled by a factor of 10 for clarity (i.e., Px10).

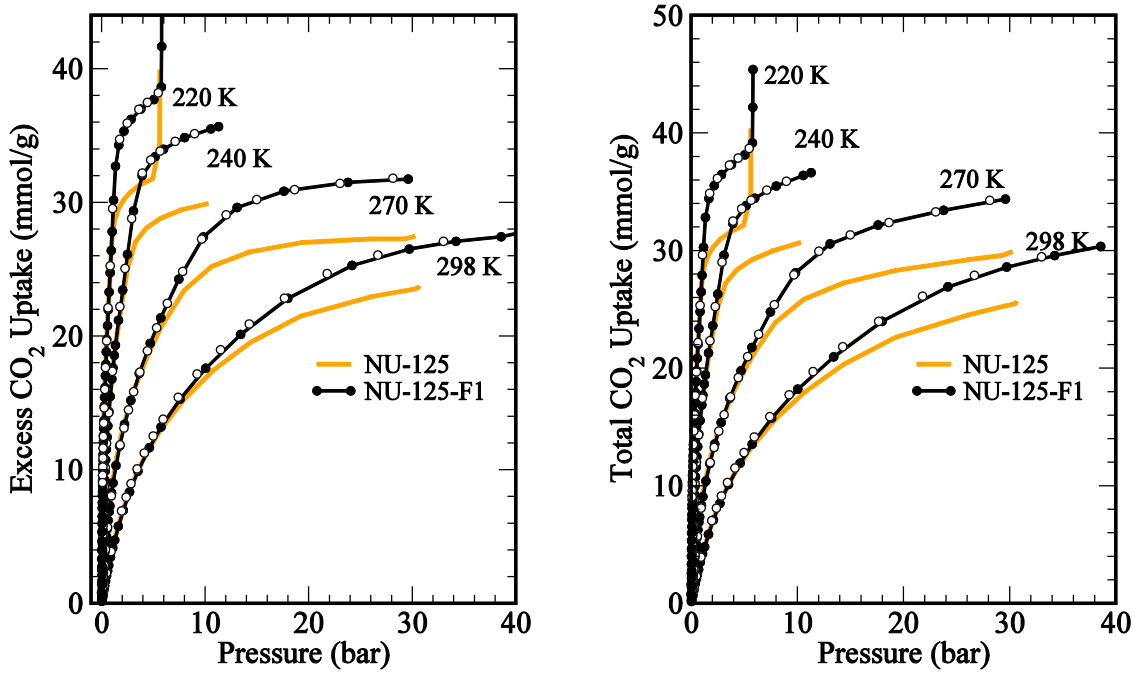

Figure S18. The gravimetric excess (left) and total (right) CO_2 isotherms at various temperatures for **NU-125-F1**. The solid and open points are adsorption and desorption isotherms using calibrated empty cell (EC) cold volumes, respectively. The orange lines in the background are the isotherms obtained from parent **NU-125** sample.

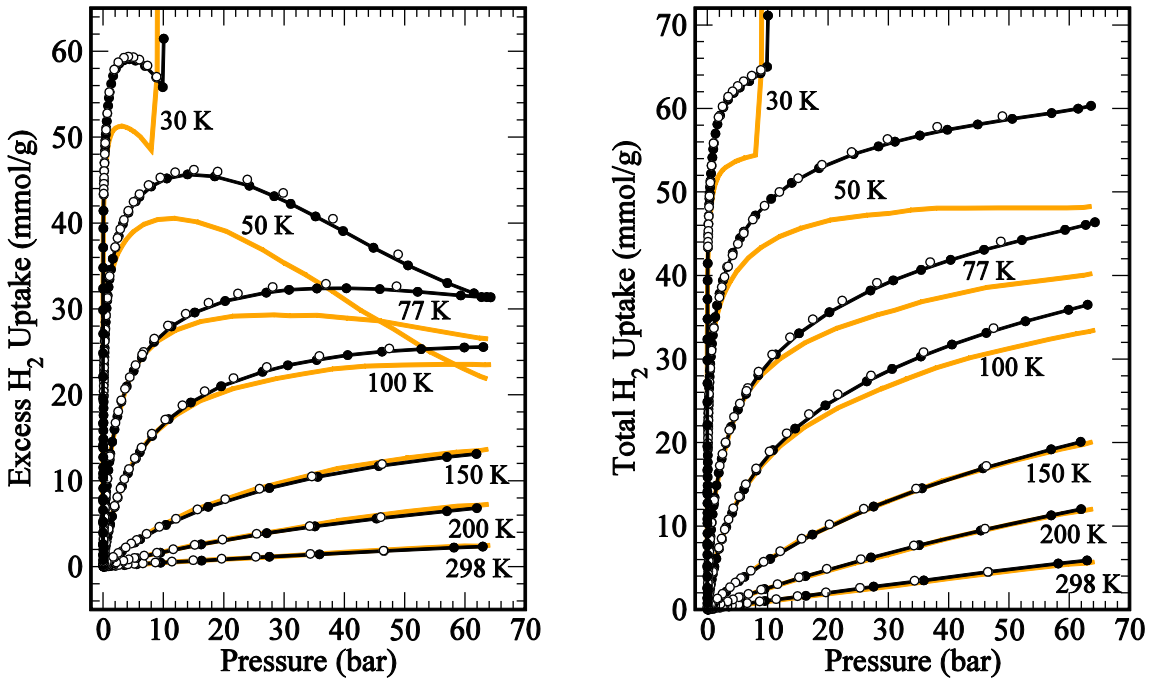

Figure S19. The excess (left) and total (right) H_2 isotherms at various temperatures for **NU-125-F1**. The solid and open points are adsorption and desorption isotherms using calibrated empty cell (EC) cold volumes, respectively. The orange lines in the background are the isotherms obtained from parent **NU-125** sample.

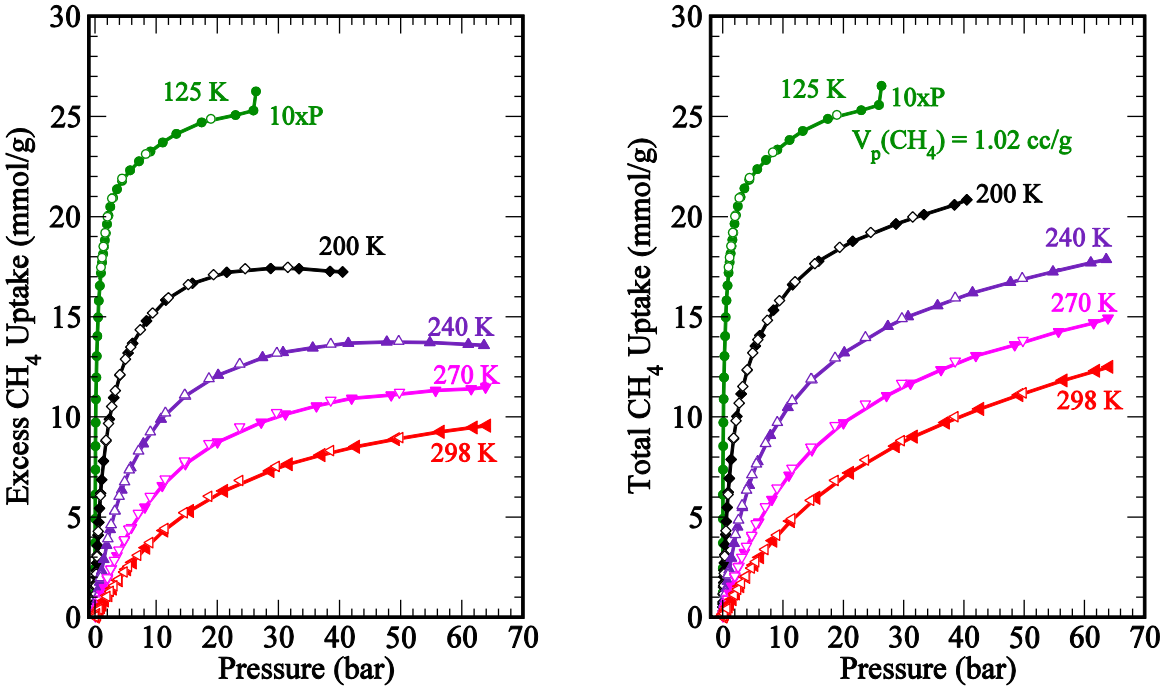

Figure S20. The gravimetric excess (left) and total (right) CH_4 isotherms at various temperatures for **NU-125-F2**. The solid and open points are adsorption and desorption isotherms using calibrated empty cell cold volumes, respectively. The pressure axes for the 125 K methane isotherms were scaled by a factor of 10 for clarity (i.e., Px10).

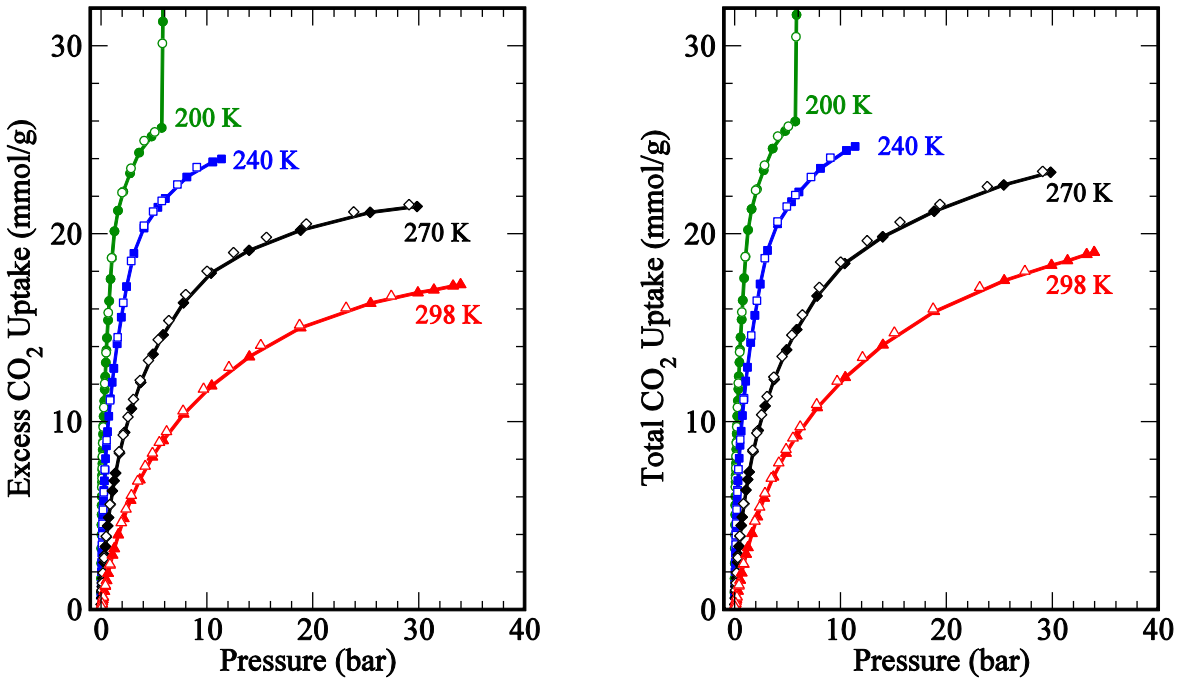

Figure S21. The gravimetric excess (left) and total (right) CO_2 isotherms at various temperatures for **NU-125-F2**. The solid and open points are adsorption and desorption isotherms using calibrated empty cell (EC) cold volumes, respectively.

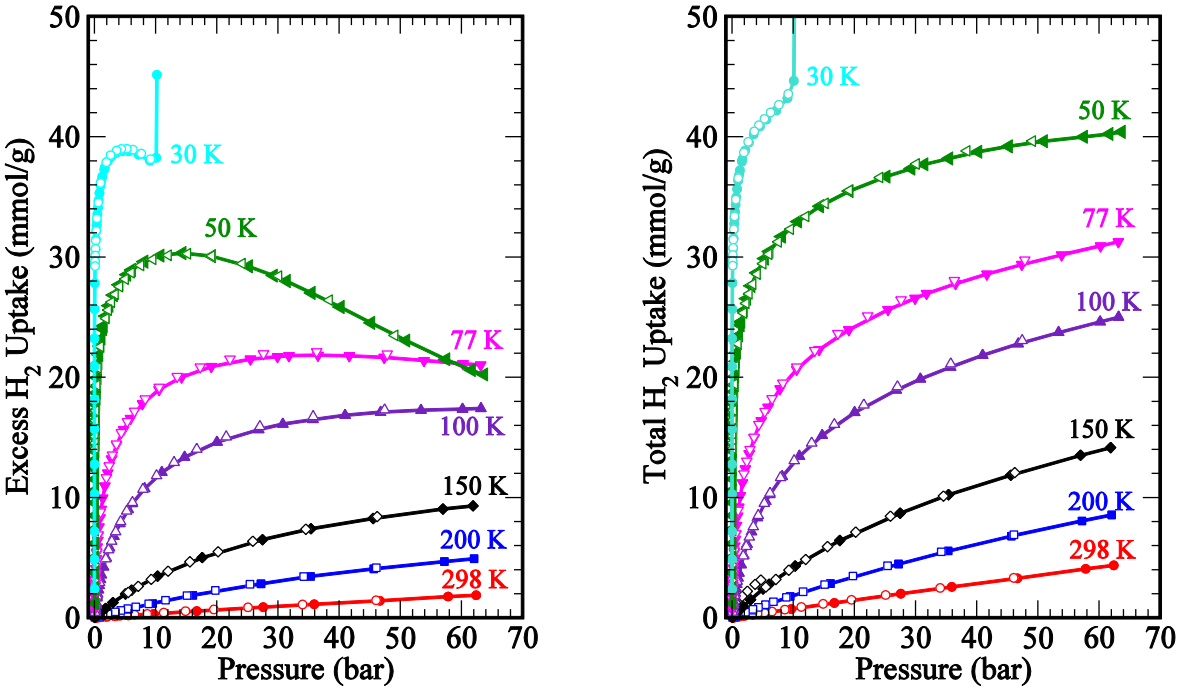

Figure S22. The excess (left) and total (right) H_2 isotherms at various temperatures for **NU-125-F2**. The solid and open points are adsorption and desorption isotherms using calibrated empty cell (EC) cold volumes, respectively.

8. Measured Isosteric Heat of Adsorption Q_{st}

Our isotherm data at a series of temperatures enable us to extract the heat of adsorption as a function of the absorbed amount as shown in the main text. The Q_{st} is calculated using the "isosteric method" where a series of isotherms were measured at a wide range of temperatures. These isotherms are then parameterized by cubic-spline which does not require any fitting and allows us to interpolate the isotherm at a constant loading. Then, the Q_{st} is obtained from the ln(P) versus 1/T plots. As an alternative to cubic-spline interpolation, we also obtain Q_{st} by fitting the isotherm data using the following form of a virial equation:

$$\ln(p) = \ln(v) + \frac{1}{T}\sum_{i=0}^{m} a_i\, v^i + \sum_{i=0}^{n} b_i\, v^i$$

where v, p, and T are the amount adsorbed, pressure, and temperature, respectively, and a_i and b_i are empirical parameters. The first four constants (i.e., a0, b0, a1, and b1) are obtained by linearizing the isotherms (1/n versus ln p) and then we increase the number of parameters gradually (two at a time) until the improvement in the fit is not significant. Usually 10 or 12 parameters are found to be enough to obtain a good fit to the isotherms. After the isotherms were fitted, by applying Clausius-Clapeyron equation, the heat of adsorption is obtained as $Q_{st} = -R\sum_{i=0}^{m} a_i v^i$ where R is the universal gas constant. As an example, below we show the isotherm data (points), cubic-spline interpolation (black lines) and the virial-fit (red lines) as well as the corresponding ln(P) versus 1/T plots and the Q_{st} from both methods along with the fit parameters a_i and b_i.

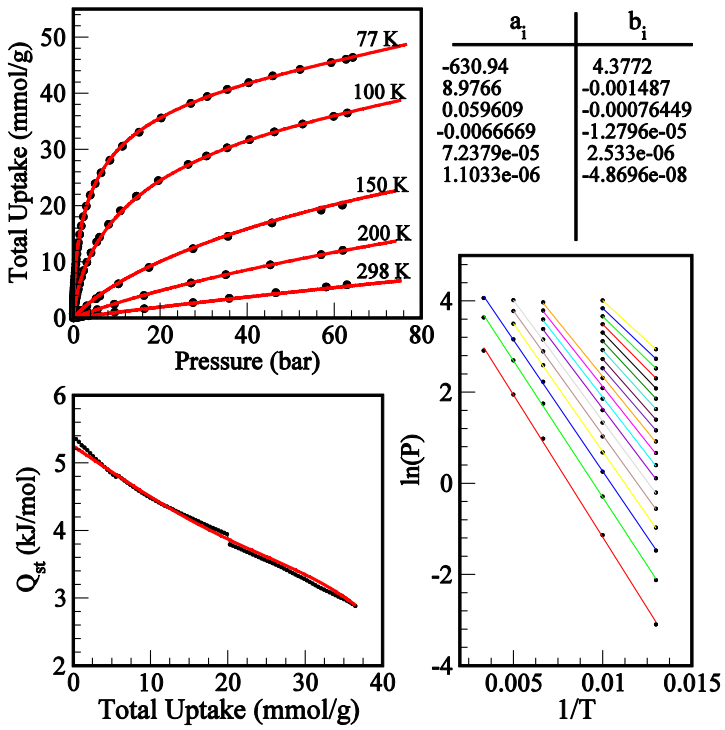

Figure S23. NU-125-F1: The H_2 adsorption isotherms (dots) and the virial fit (red-lines) along with the fit parameters as well as the Q_{st} and the ln(P)–1/T plots. The black line in the Q_{st} plot is obtained from the raw data without any virial fitting (using spline method).

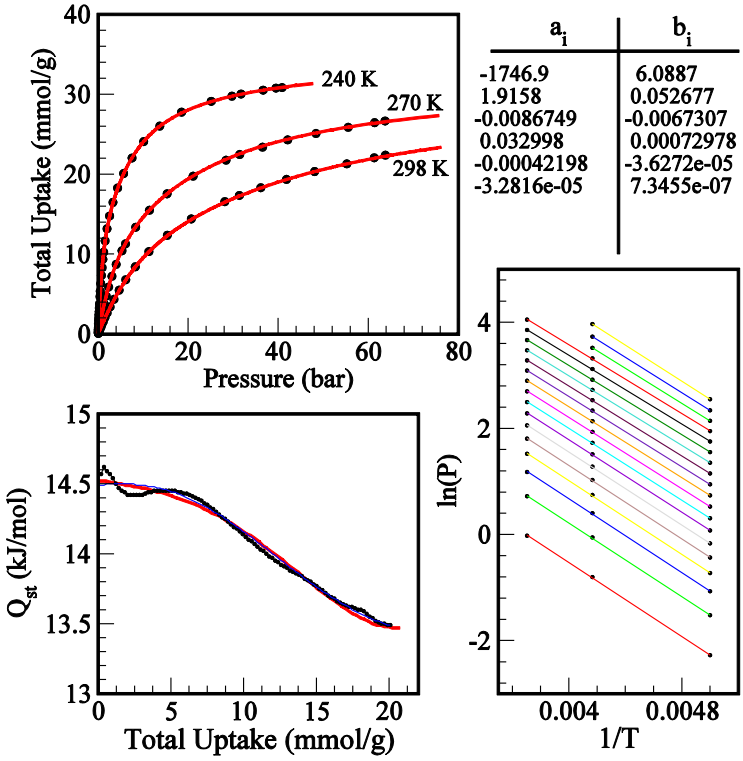

Figure S24. NU-125-F1: Same as Figure S23 but for CH_4 adsorption.

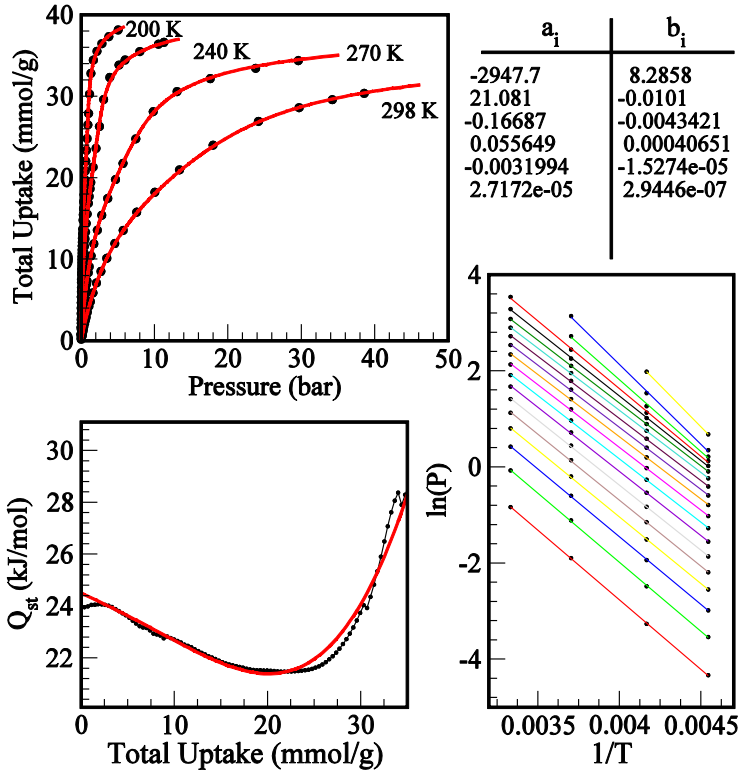

Figure S25. NU-125-F1: Same as Figure S23 but for CO_2 adsorption.

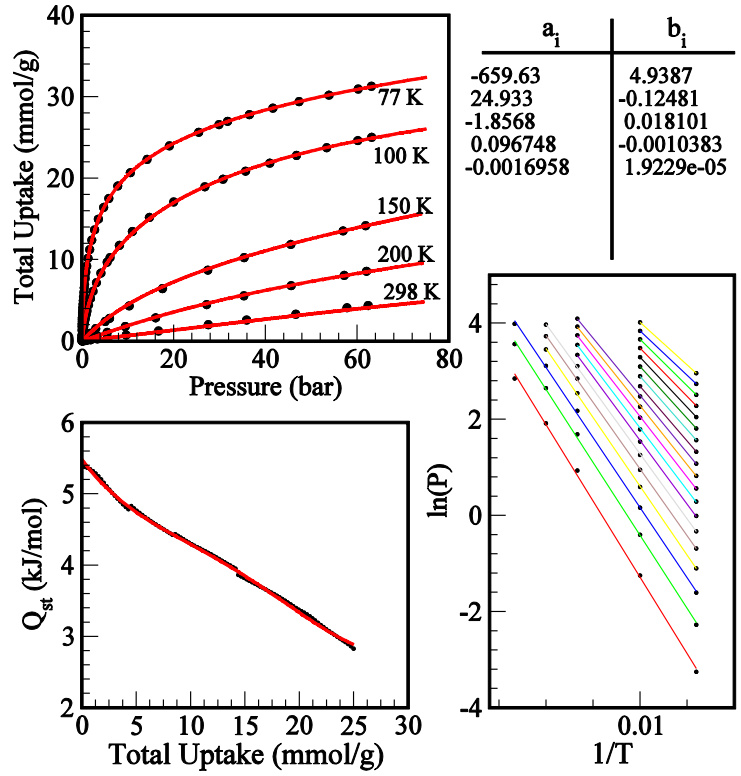

Figure S26. NU-125-F2: Same as Figure S23 but for H_2 adsorption.

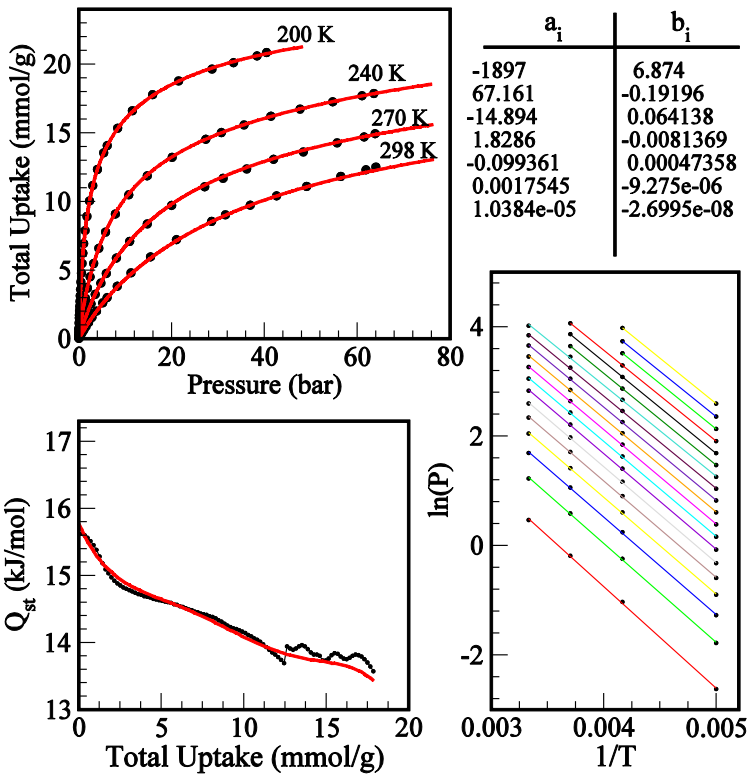

Figure S27. NU-125-F2: Same as Figure S23 but for CH_4 adsorption.

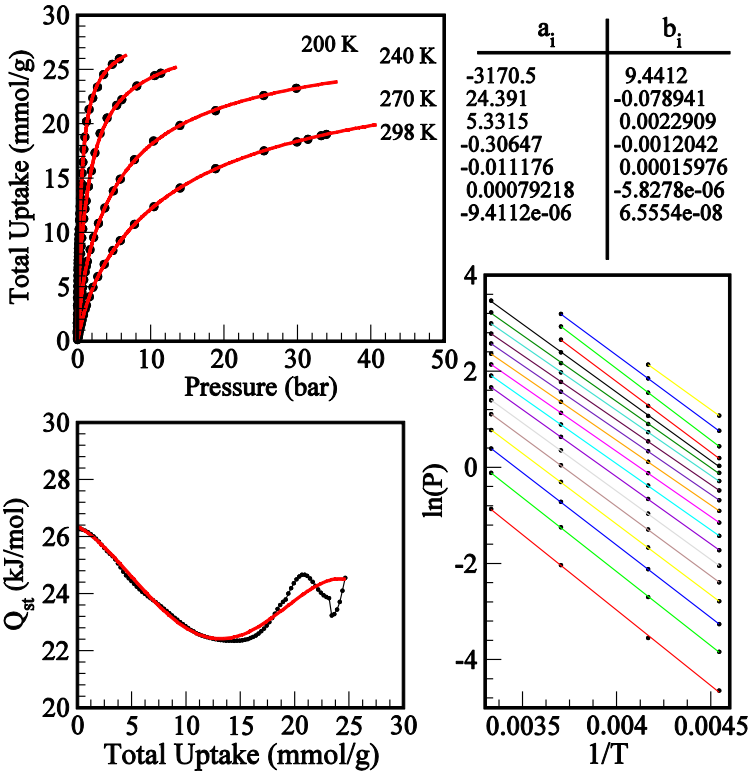

Figure S28. NU-125-F2: Same as Figure S23 but for CO_2 adsorption.

9. References

(1) Wilmer, C. E.; Farha, O. K.; Yildirim, T.; Eryazici, I.; Krungleviciute, V.; Sarjeant, A. A.; Snurr, R. Q.; Hupp, J. T. *Energy Environ. Sci.* **2013**, *6*, 1158–1163.

(2) Mao, Z.; Vakhshouri, K.; Jaye, C.; Fischer, D. A.; Fernando, R.; DeLongchamp, D. M.; Gomez, E. D.; Sauvé, G. *Macromolecules* **2013**, *46*, 103–112.

(3) Walton, K. S.; Snurr, R. Q. *J. Am. Chem. Soc.* **2007**, *129*, 8552–8556.

(4) Düren, T.; Millange, F.; Férey, G.; Walton, K. S.; Snurr, R. Q. *J. Phys. Chem. C* **2007**, *111*, 15350–15356.

(5) Zhou, W.; Wu, H.; Hartman, M. R.; Yildirim, T. *J. Phys. Chem. C* **2007**, *111*, 16131–16137.

(6) Peng, Y.; Krungleviciute, V.; Eryazici, I.; Hupp, J. T.; Farha, O. K.; Yildirim, T. *J. Am. Chem. Soc.* **2013**, *135*, 11887–11894.